JOURNAL OF MATERIALS SCIENCE 31 (1996) 2177–2186

Dielectric relaxation and electrical conduction at low field of mineral-filled epoxy

S.-L. WU*
Department of Physics, Auburn University, AL 36849, USA
I.-C. TUNG
Department of Mechanics and Materials Science, Rutgers University, P.O. Box 909, Piscataway, NJ 08855, USA

Dielectric properties and conduction of the epoxy and its composites were measured over the temperature range −20 to 70 °C and the frequency range 10^{-4}–10^{-1} Hz. Dielectric properties were obtained by performing Fourier transforms on the charging and discharging curves. The resulting isothermal frequency spectra of dielectric constants and dielectric loss factors were analysed using the Cole–Cole law to obtain the activation energy for each material. The activation energies were also obtained for isothermal d.c. current. Current density–electric field–temperature characteristics are obtained for field levels up to 60 kV cm^{-1}, with step excitation of the applied field and currents recorded after a delay time of 10 min. Current density and electric field were computed and plotted for constant temperature. The linear (ohmic) curves were obtained for fields up to about 60 kV cm^{-1} for temperatures up to about 20 °C. The non-linearity at the higher fields and temperatures did not imply the occurrence of non-ionic conduction. It has been demonstrated that both electric conduction and relaxation behaviour were ionic and could be fit by the Nakajima model for the unfilled epoxy and the Taylor model for the composites.

1. Introduction

Polyether polymers, commonly called epoxies, are widely used in a number of types of insulation systems [1], such as housings for electrical machinery and switchgear, standoff bushings in transformers, etc., primarily because of its electrically insulating properties, mechanical rigidity and toughness, chemical stability and ease of fabrication. However, epoxies exhibit a considerably low dielectric response, which limits their applications in dielectrics of coaxial cables, capacitor dielectrics, radomes, and so forth. In an attempt to avoid this disadvantage, the composite approach has been considered. As reported by Zee *et al.* [2], the dielectric constants of the epoxy composites are capable of varying in a relatively broad range by dispersing, throughout the volume of the epoxy, fine particles of a mineral which has a higher dielectric constant in comparison to the epoxy.

In the previous publication [3], the dielectric properties were studied for the epoxy and its composites containing several different volume fractions of three different dielectric fillers, using the impedance bridge method over a higher frequency region, 10^2–10^5 Hz, and the d.c. transient current method over a lower frequency region, 10^{-4}–10^{-1} Hz. It has been found that, in the high-frequency region, the relaxation behaviour is associated with the motion of the diester segments in the epoxy cross-linking network, while in the low-frequency region, the relaxation behaviour was proposed to be associated with motion of ions without the detailed analysis.

In the present study, our interest will centre around the relaxation mechanism in the low-frequency region and the conduction mechanism at low fields of the epoxy and its mineral-filled composites. It will be shown that both relaxation mechanism and electrical conduction are ionic, whether for the unfilled epoxy or the filled epoxies.

2. Theoretical models

2.1. Ionic conduction

Mass transport is direct evidence for ionic conduction of insulation systems. However, because conduction current in the insulating materials is usually small, the detection of mass transport in the systems is very difficult. In addition to mass transport of ions, ionic conduction changes with pressure, addition of appropriate ionic impurities, and electro-chemical reactions [4]. Ionic conduction in polymeric systems frequently is associated with ionic impurities or ionizable groups in the investigated material. It is thermally activated and can be modelled by a series of potential wells of depth ΔH and separation a [5]. Therefore, according

*Present address: Department of Mechanics and Materials Science, Rutgers University, P.O. Box 909, Piscataway, NJ 08855, USA.

to the rate process theory [6], in the absence of an external field and at atmospheric pressure, the jumping rate (w, jump number per unit time) for an ion in a certain equilibrium position to either neighbouring equilibrium position is given by

$$w = \nu_0 \exp\left(-\frac{\Delta H}{kT}\right) \quad (1)$$

where ν_0 is the vibrational frequency of the ions in the potential well, ΔH is the energy barrier for ionic movement, k is the Boltzmann constant and T is the absolute temperature.

When a negative ion moves from one equilibrium position to another in the presence of a uniform electric field, E, the potential energy of the ion increases by $eEa/2$ upon movement in the field direction, and decreases by that amount in the opposite direction, where e is the charge. Thus, the jumping rate for ions in the field direction, w_+, and in the opposite direction, w_-, are, respectively

$$w_+ = \nu_0 \exp\left[-\frac{\Delta H - (eEa/2)}{kT}\right] \quad (2)$$

and

$$w_- = \nu_0 \exp\left[-\frac{\Delta H + (eEa/2)}{kT}\right] \quad (3)$$

The mean drift velocity (in the direction of positive current) is therefore given by

$$u = a(w_+ - w_-) = 2a\nu_0 \sinh\frac{eEa}{2kT} \exp\frac{-\Delta H}{kT} \quad (4)$$

At low field strengths, $kT \gg eEa$ ($E \gg 10\ \mathrm{kV\ cm^{-1}}$ at 300 K), the hyperbolic term in Equation 4 is approximately $eEa/2kT$. So the mean drift velocity at low field strengths can be expressed as

$$u = \frac{eEa^2\nu_0}{kT} \exp\frac{-\Delta H}{kT} \quad (5)$$

Accordingly, the mobility, μ, and the conductivity, σ, for ionic conduction at low fields are

$$\mu = \frac{u}{E} = \frac{ea^2\nu_0}{kT} \exp\frac{-\Delta H}{kT} \quad (6)$$

and

$$\sigma = neu = \frac{ne^2a^2\nu_0}{kT} \exp\frac{-\Delta H}{kT} \quad (7)$$

where n is the density of ions. Equation 7 can be written

$$\sigma = \sigma_0 \exp\frac{-\Delta H}{kT} \quad (8)$$

where σ_0 is the pre-exponential coefficient with the value $ne^2a^2\nu_0/kT$, so it is related to the density of ions, n, hopping distance, a, and the absolute temperature, T.

2.2. The relation of ΔH between a.c. and d.c. measurements

2.2.1. Taylor model

Charles [7] found, whenever the relaxation process is due to ionic conduction, that the same ionic species is also implicated in the d.c. conduction process, and the activation energy for d.c. conduction is generally greater than that for a.c. conduction. Based on this concept, Taylor [8] suggested a model wherein the ionic conduction involves a random distribution of potential barriers of different heights, as depicted in Fig. 1. All the ions may oscillate within the distance a, under the smaller potential barriers for a.c. conduction and therefore give rise to a characteristic frequency that corresponds to a relaxation time for a specific temperature. When a d.c. voltage is applied, where current paths through the entire dielectric must be transversed, conduction is limited by the barriers that are the highest along such paths. Thus, the activation energy for d.c. conduction is that of the highest barriers along conduction paths.

2.2.2. Nakajima model

In order to explain the relationship between the d.c. conductivity, σ, and the a.c. relaxation time, τ, for ionic conduction, Nakajima [9] suggested a more realistic model based upon the assumption that the ionic migration jumps follow a zigzag path, instead of an idealized one-dimensional path. The other assumptions, in order to simplify the problem, are equal jump a and equal potential height ΔH. The zigzag motion of the ions is described in Fig. 2. Let ϕ be the angle between the axis of the jump path and the applied field, and θ the angle between the path axis and the actual jump direction. When the field is applied, as

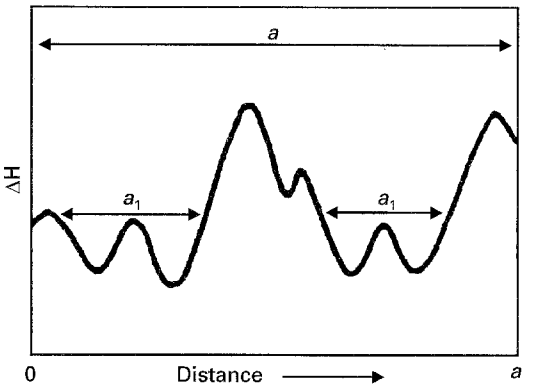

Figure 1 Randomly distributed potential energy diagram suggested by Taylor.

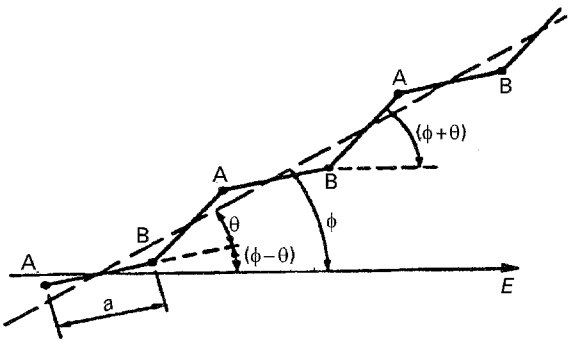

Figure 2 A zigzag transition by the Nakajima model. Path direction is indicated by the broken line.

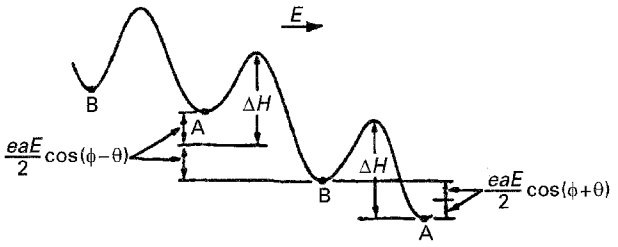

Figure 3 Potential energy diagram for a positive ion in the presence of an applied field.

clearly shown in Fig. 3, the distribution of potential barriers becomes quite different from that in the Taylor model. After following the treatment of Nakajima, the average current, I_{ave}, is obtained

$$I_{ave} = \frac{Ne^2a^2wE}{6kT}[1 + \exp(-4wt)] \quad (9)$$

The average current, I_{ave} is contributed by, according to Equation 9, the steady state d.c. conduction current, the first term on the right, and the polarization current, the second term. The quantity, $4w$, in the exponent is the reciprocal of τ, the Debye relaxation time. In order to find to conductivity, σ, of an ionic-dominated material, N is substituted by n, where n is the number of ions involved per volume ($= N/Ad$, A is the area and d the thickness of a material). Thus, the conductivity, σ, from Equation 9, can be expressed as

$$\sigma = \frac{J_{ave}}{E} = \frac{ne^2a^2dw}{6kT} = \frac{ne^2a^2d}{24kT\tau} \quad (10)$$

The change in dielectric constant due to the above process, $\varepsilon_s - \varepsilon_\infty$, can be found by integrating the polarization term of Equation 9 from $t = 0$ to $t = \infty$. We obtain

$$\varepsilon_s - \varepsilon_\infty = \frac{ne^2a^2wd}{6\varepsilon_0kT}\int_0^\infty \exp(-4wt)\,dt = \frac{ne^2a^2d}{24\varepsilon_0kT} \quad (11)$$

where ε_s (static dielectric constant) and ε_∞ are the dielectric constants at the low and high-frequency ends of the polarization transition, respectively. Equations 10 and 11 can be combined and the relationship between the conductivity, σ, and the relaxation time, τ, under the assumptions of Nakajima, can be expressed as

$$\sigma = \frac{\varepsilon_0(\varepsilon_s - \varepsilon_\infty)}{\tau} = 2\pi f_m\varepsilon_0(\varepsilon_s - \varepsilon_\infty) \quad (12)$$

where f_m is the characteristic frequency. Equation 12 shows the number of ions contributing to the relaxation behaviour equals those contributing to the conduction current.

3. Experimental procedure

3.1. Materials

The resin/hardener system used throughout was a mixture of Epon 828 (Shell Chemical Co.), NMA (nadic methyl anhydride) and BDMA (benzyldimethylamide) with the weight ratio 100:85:0.5, in which NMA and BDMA served as the curing agent and accelerator, respectively.

The three fillers used were ceramic materials, having low dielectric loss and the nominal dielectric constants of 6, 16 and 50 in the microwave region. These are designated commercially as ATD-6, ATD-16 and ATD-60, and supplied by Ampex Co. ATD-6 is the mineral fosterite with the density 2.9 g cm^{-3}, which is primarily $MgSiO_3$ with less than 10% magnesium replaced by iron. The composition of ATD-16 is $MgTiO_3$ with the density 3.4 g cm^{-3} and that of ATD-50 is single-crystal compound $BaTiO_{11}$ (80% TiO_2 sintered with 20% $BaTiO_3$), with the density 4.4 g cm^{-3}. The average particle size for these fillers is ~ 3 μm and particle shapes are roughly spherical.

3.2. Sample preparation

The calculated amounts of the properly dried filler, either 30% or 40% volume fraction, were mechanically mixed with the resin system at 80 °C until a homogeneous mixture was obtained. The mixture was heated to 120 °C in a vacuum oven and degassed by a periodic air flushing process. The homogeneous and degassed mixture was then poured into the glass moulds coated with a thin film of a mould-release agent and allowed to curve in a vacuum oven. The curing was carried out at 121 °C for 2 h and subsequently 204 °C for 2 h at atmospheric pressure. Then the casts were cooled overnight to room temperature at a reduced pressure. The resulting casts obtained were cylindrical rods approximately 15 cm long and 4 cm diameter. Those cylindrical rods of the casts were cut into the proper sizes of the specimens. After final polishing of the specimens with 1.0 μm diamond paste suspended in oil, the silver paint (Conductor Composition 4929 from DuPont Company) was coated on the specimens and allowed to cure at 55 °C for 2 h for electroding purposes.

3.3. Measurements

3.3.1. D.c. transient current method

In this method, the specimen and electrode configurations are shown in Fig. 4, in which the disc specimen is 3.81 cm diameter and ~ 0.5 mm thick. On the top surface of the specimen, a circular silver-painted pattern, 1.27 cm diameter, is coated but not shown in Fig. 4. As observed, the surface area of the specimen is much larger than that of the electrodes, thereby avoiding surface conduction. The measuring process is as follows. First, a constant step voltage 2 kV with a duration of 170 min was applied by the power supply (Monroe Electronics Model Coronaply II) to the specimen, during which the specimen was charged. At the same temperature, after the voltage step was completed and the specimen was short-circuited, during which the specimen was discharged. The charging and discharging currents through the specimen were measured every 5 s by the Keithley 610C electrometer, which had a low-impedance analogue output that was

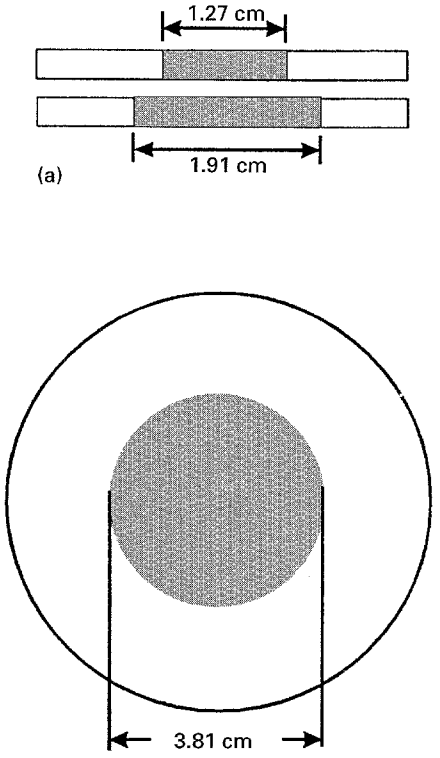

Figure 4(a) Configuration of the electrodes (shaded area in cross-sectional view) for the d.c. transient current method. (b) Silver-painted pattern (shaded area) on the bottom surface of the specimen.

digitized by the Keithley 195A multimeter. The charging and discharging currents, after level-off, were $\sim 10^{-14}$ A, which approached the lowest measurable current on the electrometer. Therefore, in this regime, care must be taken to avoid the noise due to the mechanical vibrations of the equipment. Also, due to the limitation of response time in the equipment, a delay of 10 s was inserted before the first current reading was recorded.

Then, the values of ε' and ε'' were calculated, from the discharging current curves only, following a method formulated by Block *et al.* [10]

$$\varepsilon'(\omega) - \varepsilon(\infty) = \frac{1}{C_0 V_0} \int_0^\infty i(t) \cos(\omega t)\, dt \quad (13)$$

$$\varepsilon''(\omega) = \frac{1}{C_0 V_0} \int_0^\infty i(t) \sin(\omega t)\, dt \quad (14)$$

where C_0 is the vacuum capacitance of the capacitor, V_0 the applied step voltage, $i(t)$ the discharging current, and ω the angular frequency.

3.3.2. D.c. I V T measurements

The configurations of the specimen and electrodes are the same as those for the d.c. transient current method. Step voltages were applied and the currents were measured 10 min after applying each voltage step. The measurements were performed with relative humidity less than 25% at temperatures from -20 to 60 °C. It may be noted that the currents at the temperatures below -30 °C could not be distinguished from noise, so the data obtained at these temperatures were meaningless.

4. Results

4.1. D.c. transient method

Five specimens were used, whose compositions and thicknesses are shown in Table I. After the steady current of each charging current curve was determined by taking the average of the last 100 current data, the conductivity could be calculated from the dimensions of the specimen, current and amplitude of the voltage step for each corresponding temperature. When plots of log(conductivity) versus 1000/temperature are made for each composition, straight lines are obtained, indicating the presence of an Arrhenius relationship and thermal activation energy. The activation energy for d.c. conduction is obtained from the slope of the graph of log(conductivity) versus 1000/temperature, based on Equation 8. The calculated activation energy for each composition is also shown in Table I.

In order to analyse the relaxation behaviour in the frequency range 10^{-4}–10^{-1} Hz, the isothermal dielectric properties of the materials were obtained by taking the Fourier transform of the discharging current curves [3, 11], according to Equations 13 and 14. For the Cole–Cole law [12] to be considered, the complex dielectric constant can be represented as

$$\varepsilon^* = \varepsilon_\infty + \frac{\varepsilon_s - \varepsilon_\infty}{1 + (i\omega\tau)^{1-\alpha}} \qquad 0 \le \alpha \le 1 \quad (15)$$

Further, Equation 15 can be separated into the real and imaginary parts

$$\varepsilon'(\omega) = \varepsilon_\infty + \frac{1}{2}(\varepsilon_s - \varepsilon_\infty) \times \left\{1 - \frac{\sinh[(1-\alpha)\ln\omega\tau]}{\cosh[(1-\alpha)\ln\omega\tau] + \sin\frac{1}{2}\alpha\pi}\right\} \quad (16)$$

$$\varepsilon''(\omega) = \frac{1}{2}(\varepsilon_s - \varepsilon_\infty)\left\{\frac{\cos\frac{1}{2}\alpha\pi}{\cosh[(1-\alpha)\ln\omega\tau] + \sin\frac{1}{2}\alpha\pi}\right\} \quad (17)$$

TABLE I Compositions and thicknesses of specimens for the d.c. transient current method and their calculated activation energies for d.c. conduction during charging

	Unfilled epoxy	Epoxy + 40% ATD-6	Epoxy + 40% ATD-16	Epoxy + 30% ATD-50	Epoxy + 40% ATD-50
Thickness (mm)	0.635	0.610	0.444	0.381	0.533
Activation energy[a] (eV)	0.645	0.378	0.602	0.483	0.568

[a]For d.c. conduction during charging.

When $\alpha = 0$, Equation 15 reduces to the Debye equation. The coefficient α is a measure of the deviation from the Debye equation. The calculated results, yielding $\varepsilon_s - \varepsilon_\infty$, α, τ_m and maximum loss, i.e. $\varepsilon''(\tau_m)$, at the different temperatures for each material are shown in Tables II–VI, where τ_m is the relaxation time. As shown in Fig. 5, the graph of $\log \tau_m$ versus $1000/T$ for each material is also found to be linear, so that the Arrhenius equation is satisfied, as follows

$$\tau = \tau_0 \exp\left(\frac{\Delta H}{kT}\right) \quad (18)$$

where ΔH is the thermal activation energy to relaxation and τ_0 is constant. Accordingly, the activation energy for each material is calculated and also shown in Table II–VI.

4.2. D.c. I–V–T measurements

The compositions and thicknesses of the four specimens for the d.c. I–V–T (current–voltage–temperature) measurements are (1) unfilled epoxy, 0.635 mm, (2) epoxy/40% ATD-6, 0.610 mm, (3) epoxy/40% ATD-16, 0.444 mm, (4) epoxy/40% ATD-50, 0.533 mm.

Figs 6–9 show the current density versus applied electric field for each specimen under isothermal conditions. The results show, for all the test specimens,

TABLE II Dielectric properties for unfilled epoxy

Temperature (°C)	ε_s–ε_∞	ε_s	ε_∞	α	Max. loss	τ_m(s)
10	0.48	4.49	4.01	0.491	0.101	35210
20	0.60	4.72	4.12	0.399	0.152	7678
30	0.89	5.08	4.19	0.297	0.271	2785
40	1.25	5.53	4.28	0.275	0.400	1125

Activation energy = 0.684 eV

TABLE III The dielectric properties for epoxy/40% ATD-6

Temperature (°C)	ε_s–ε_∞	ε_s	ε_∞	α	Max. loss	τ_m(s)	f_m(Hz)
−20	0.64	5.85	5.21	0.559	0.145	6002.0	2.65×10^{-5}
−10	0.73	5.99	5.26	0.520	0.148	4189.5	3.80×10^{-5}
0	0.91	6.20	5.29	0.513	0.184	3491.1	4.56×10^{-5}
10	1.17	6.51	5.34	0.475	0.235	2975.0	5.35×10^{-5}
20	1.79	7.16	5.37	0.435	0.426	2415.7	6.59×10^{-5}
30	2.60	8.01	5.41	0.417	0.640	2295.0	6.93×10^{-5}
40	3.70	9.15	5.45	0.376	0.986	1532.6	1.04×10^{-4}
50	4.27	9.77	5.50	0.369	1.101	1147.1	1.39×10^{-4}

Activation energy = 0.151 eV

TABLE IV The dielectric properties for epoxy/40% ATD-16

Temperature (°C)	ε_s–ε_∞	ε_s	ε_∞	α	Max. loss	τ_m(s)	f_m(Hz)
−10	0.56	8.07	7.51	0.525	0.101	3851.0	4.13×10^{-5}
0	0.69	8.26	7.57	0.494	0.145	3526.2	4.51×10^{-5}
10	1.03	8.66	7.63	0.435	0.244	2805.1	5.67×10^{-5}
20	1.59	9.27	7.68	0.399	0.437	2245.0	7.09×10^{-5}
30	1.92	9.65	7.73	0.384	0.505	1993.7	7.98×10^{-5}
40	3.59	11.37	7.78	0.355	0.996	1495.0	1.06×10^{-4}
60	6.96	14.83	7.87	0.348	1.609	1683.4	9.45×10^{-5}

Activation energy = 0.135 eV

TABLE V Dielectric properties for epoxy/30% ATD-50

Temperature (°C)	ε_s–ε_∞	ε_s	ε_∞	α	Max. loss	τ_m(s)
−10	0.84	11.26	10.42	0.464	0.189	4107.0
0	0.83	11.32	10.49	0.429	0.200	3489.9
10	1.59	12.16	10.57	0.395	0.410	2697.1
20	2.13	12.78	10.65	0.369	0.643	1889.5
30	3.12	13.85	10.73	0.348	0.879	1485.7
60	4.42	15.34	10.92	0.351	1.235	812.0

Activation energy = 0.182 eV

TABLE VI Dielectric properties for epoxy/40% ATD-50

Temperature (°C)	$\varepsilon_s-\varepsilon_\infty$	ε_s	ε_∞	α	Max. loss	τ_m(s)
10	1.59	14.16	12.57	0.350	0.452	4125.5
20	1.67	14.31	12.64	0.251	0.585	2592.5
30	1.86	14.56	12.70	0.153	0.619	1453.1
40	1.98	14.76	12.78	0.132	0.830	903.5
50	2.23	15.07	12.84	0.123	0.920	713.5
60	2.75	15.62	12.87	0.103	1.171	685.1

Activation energy = 0.316 eV

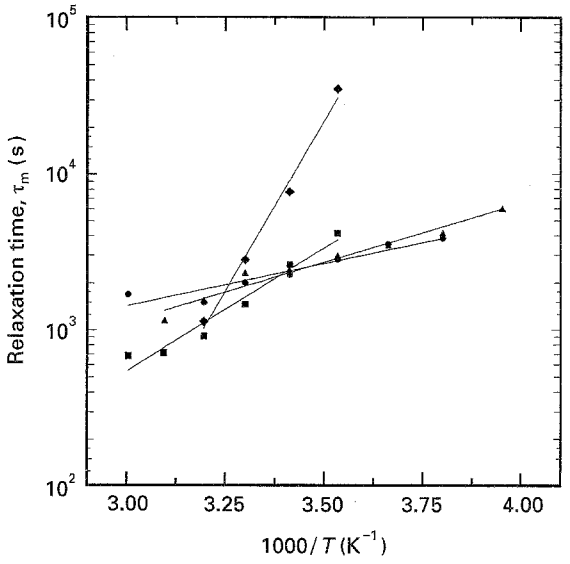

Figure 5 Log(relaxation time) versus 1000/T for (◆) unfilled epoxy, (▲) epoxy/40% ATD-6, (●) epoxy/40% ATD-16 and (■) epoxy/40% ATD-50.

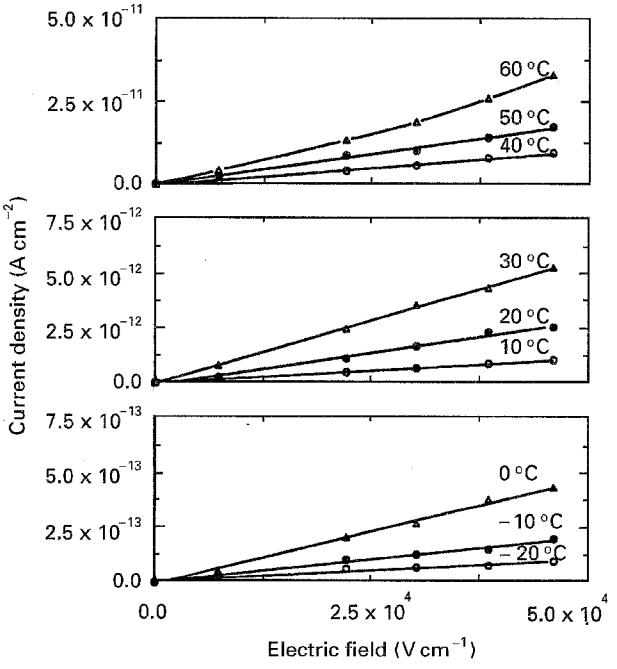

Figure 6 Current density versus applied field for unfilled epoxy under isothermal conditions.

that Ohm's law is obeyed for the electric field levels below 6×10^4 V cm^{-1} for temperatures up to 30 °C, in 10 °C intervals. However, when temperature was increased to 60 °C, all graphs show the current density rising with its slope increasing with field and with

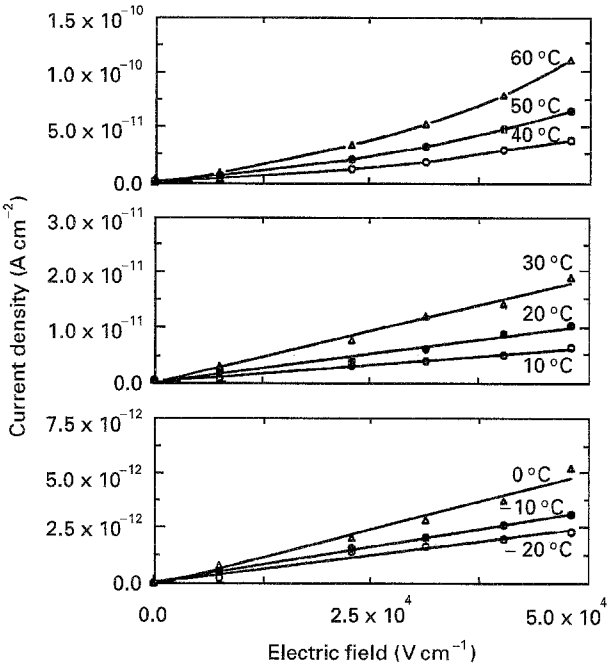

Figure 7 Current density versus applied field for epoxy/40% ATD-6 under isothermal conditions.

temperature. The graphs indicate that the non-linearity is introduced at a lower temperature for the filled materials than for the pure epoxy resin itself, because the non-linearity appears at 40 °C for the filled materials, but at 60 °C for the unfilled epoxy resin.

The graph of log(conductivity) versus 1000/T for each specimen is shown in Fig. 10, where the conductivity for each temperature and specimen is calculated from the slope of each of the isothermal lines. The activation energies of the conduction with a 10 min charging period, calculated from the slopes of log (conductivity) and 1000/T, are 0.650, 0.303, 0.450 and 0.313 eV for unfilled epoxy, epoxy/40% ATD-6, epoxy/40% ATD-16 and epoxy/40% ATD-50, respectively.

5. Discussion

Referring to Tables II–VI, the frequency relaxation data lead to dielectric loss factors that increase two to four times in going from the unfilled to filled materials at the testing temperatures. As the test temperature increases, this particular relaxation peak moves towards higher frequencies. Also, α in the Cole–Cole law decreases as temperature increases, which means behaviour is more Debye-like as the temperature

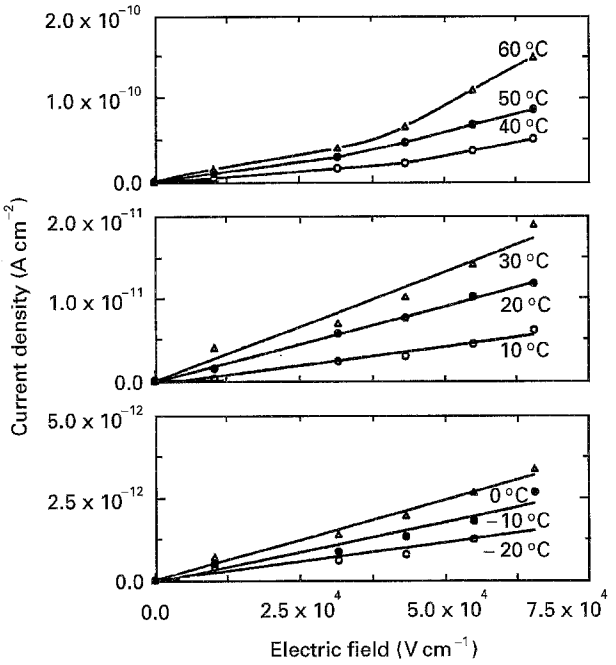

Figure 8 Current density versus applied field for epoxy/40% ATD-16 under isothermal conditions.

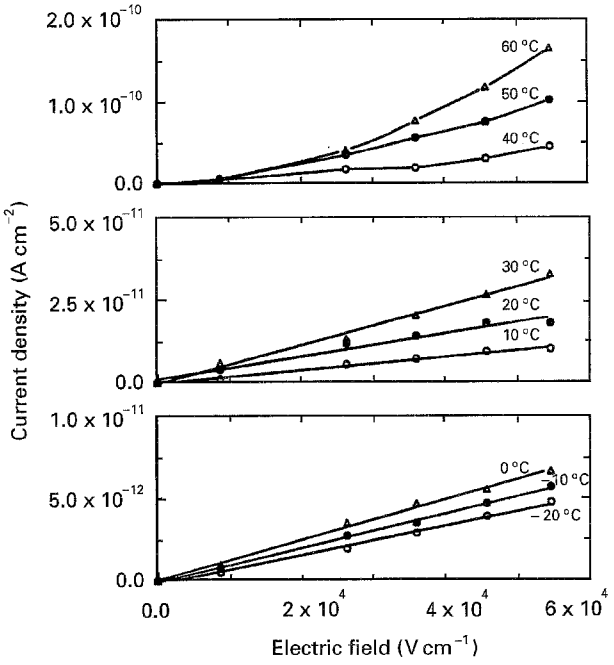

Figure 9 Current density versus applied field for epoxy/40%ATD-50 under isothermal conditions.

increases ($\alpha = 0$ for Debye behaviour), as indicated in Tables II–VI.

As is well known, both polarization and d.c. conduction contribute to dielectric loss. "Real" dielectric loss, $\varepsilon''_{real}(\omega)$, which is associated with the charging current with step excitation, can be expressed as

$$\varepsilon''_{real}(\omega) = \varepsilon''_{pol}(\omega) + \varepsilon''_{d.c.} = \varepsilon''_{pol}(\omega) + \frac{\sigma}{\omega\varepsilon_0} \quad (19)$$

where ε''_{pol} is dielectric loss obtained from the Fourier transform of the discharging polarization current, ε''_{real} is obtained from the Fourier transform of the charging

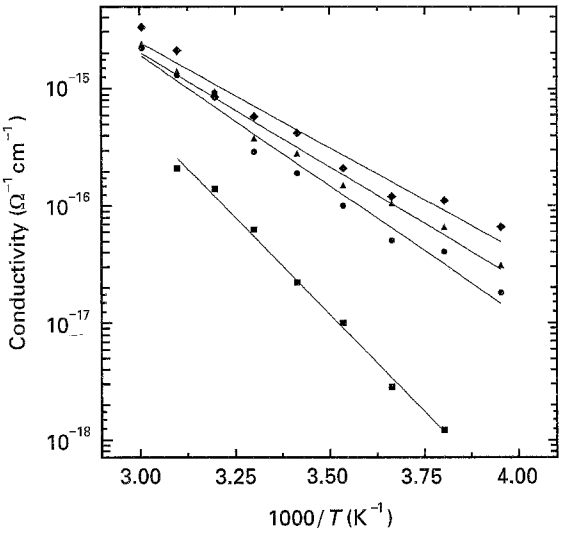

Figure 10 Log(conductivity) versus 1000/T for (■) unfilled epoxy, (▲) epoxy/40% ATD-6, (●) epoxy/40% ATD-16 and (◆) epoxy/40% ATD-50.

current (including both polarization and d.c. conduction components), ε_0 is the permittivity of a vacuum with a value of 8.85×10^{-12} F m^{-1} in SI units and σ is the conductivity from Tables II–VI. The frequency spectra of real dielectric loss and dielectric loss due to polarization at – 20 and 40 °C for epoxy/40% ATD-16, derived from the charging and discharging current, are shown in Fig. 11. In this figure it can be clearly seen that, as frequency decreases, dielectric loss due to d.c. conduction becomes the dominant term. At the lower temperatures, dielectric loss due to d.c. conduction is comparable to that due to polarization effects. However, as temperature rises, d.c. conductivity approximately increases 2–15 times for a 30 °C rise in temperature, so that dielectric loss due to d.c. conduction current becomes much more dominant. Although only ε''_{real} and ε''_{pol} are illustrated for epoxy/40% ATD-16, their trends are the same for all the other specimens. The mechanisms of the polarization (contributing to ε''_{pol}) and d.c. conduction (contributing to $\varepsilon''_{d.c.}$) associated with the relaxation behaviour in the low frequency range are discussed below.

5.1. Dielectric relaxation and conduction mechanism for unfilled epoxy

It has been reported [13, 14] that the electrical conduction of the epoxies (note the curing agents used in their studies differ from that used in ours) at low fields is dominated by the motion of ions. We hypothesize that the d.c. conduction mechanism and the relaxation at high temperatures and at peak frequencies somewhat less than 10^{-4} Hz for the epoxy, are ionic in this study. To test this hypothesis, the relaxation times are calculated using Equation 12 from the Nakajima model with the measured temperature dependence of the experimental d.c. conductivity (see Table I) and extrapolation of experimental data using the Cole–Cole law to obtain $\varepsilon_s \sim \varepsilon_\infty$ as a function of temperature (see Table II). These Nakajima relaxation times are then compared with the relaxation times

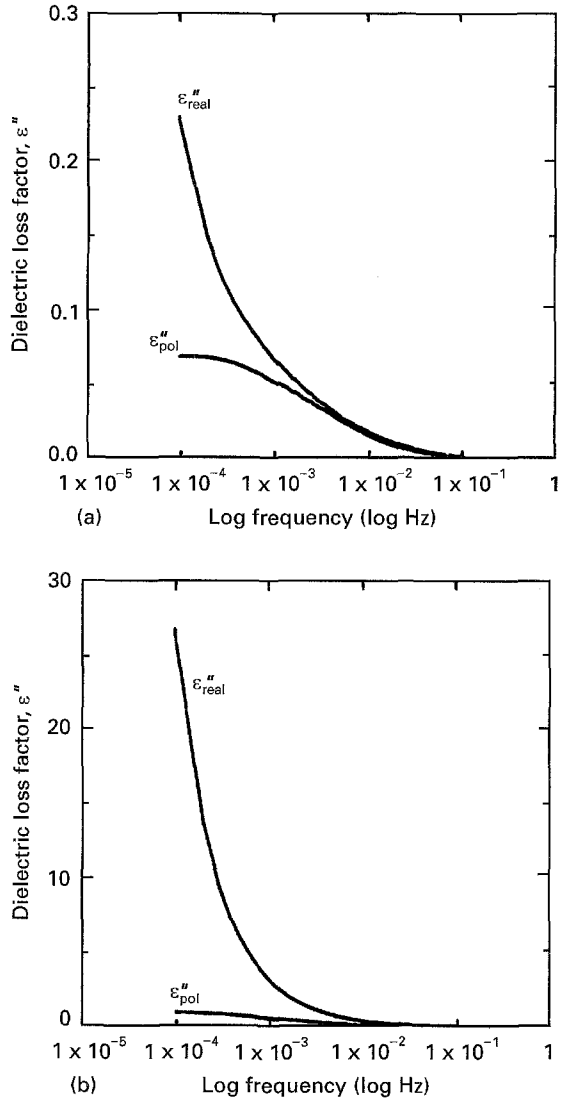

Figure 11 Real and polarization dielectric loss factors of epoxy/40% ATD-16 versus log(frequency) at temperatures of (a) – 20 and (b) 40 °C.

calculated from Cole–Cole law (see Table II). If the Nakajima relaxation times are equal those obtained through the the Cole–Cole equations at each temperature, we should conclude that the polarization and conduction mechanisms at very low frequencies are ionic for the epoxy. The detailed calculation follows.

We have found that the activation energies of the unfilled epoxy are $\Delta H_{a.c.} = 0.684$ eV (from the slope of $\ln\tau$ versus $1/T$ see Table II), $\Delta H_{d.c.} = 0.645$ eV (from the slope of $\ln\sigma$ versus $1/T$, see Table I) and $\Delta H_{10\,min} = 0.650$ eV (from the slope of $\ln\sigma$ versus $1/T$, see Fig. 8). As mentioned in the Section 2 for a particular conduction mechanism under a.c. excitation, the activation energy is smaller than or equal to that for d.c. excitation, according to the Taylor or Nakajima model. Because $\Delta H_{a.c.}$ (for the relaxation in this low-frequency range) and $\Delta H_{d.c.}$ are taken as equal for the unfilled epoxy, the characteristic frequency, f_m, for the relaxation in the low-frequency range at each temperature can be calculated from Equation 12 by the Nakajima model. Table VII shows the calculated characteristic frequencies from the Nakajima model, $f_{m,N}$, those obtained from the Cole–Cole analyses, $f_{m,C-C}$, at the temperatures of 10–40 °C and the ratio $f_{m,N}/f_{m,C-C}$ at each temperature. The ratios $f_{m,N}/f_{m,C-C}$ at 10 and 20 °C, in the last column of Table VII, are 6.1 and 2.3, respectively. These high values may be due to distortion of the Cole–Cole plots by the intrusion of an additional relaxation at the higher frequency/lower temperature region. However, the ratios at 30 and 40 °C are 1.4 and 0.8, respectively. These are close to unity, in accord with the hypothesis. Thus, the low-frequency (10^{-4}–10^{-1} Hz) relaxation behaviour at the temperatures of 10–40 °C and conduction behaviour of the unfilled epoxy are both due to the motion of ions and these ions follow zigzag paths (as predicted by the Nakajima model). As is usually the case, these ions may come from contamination effects, such as residual solvents, catalyst or unreacted monomers.

5.2. Dielectric relaxation and conduction mechanism for filled epoxies

When 40% filler was added to the pure epoxy resin, the conductivities of the composites at 20 °C were found to increase only two to seven times, compared with that of the unfilled epoxy at the same temperature (see [3]). The conductivities of the epoxy, pure ATD-6 in the form of a sintered disc, and epoxy/40% ATD-6 at 20 °C are 1.58×10^{-17}, 2.62×10^{-11} and 4.13×10^{-17} $(\Omega\,\text{cm})^{-1}$, respectively. Thus, embedding the particles of the filler into the epoxy resin did not change the conductivity by an amount commensurate with the added carrier density of the filler, considering that the conductivity of pure ATD-6 is six orders higher than that of the unfilled epoxy. To understand the low conductivity of the composite, the electron hopping mechanism, hypothesized in the ATD-6 and associated with transition metal oxides [15], must be blocked at the filler–epoxy interfaces in epoxy/40% ATD-6. In such a case, the electron movement in each particle contributes a Maxwell–Wagner polarization mechanism, but does not add to the carrier density in the epoxy matrix. This polarization is in the same sense as that of the other polarization and causes a decrease in the electric field within the particles and

TABLE VII Characteristic frequencies calculated from the Cole–Cole analyses and Nakajima model at temperatures of 10–40 °C and the ratios for unfilled epoxy

Temperature (°C)	$f_{m,C-C}$(Hz) (Cole–Cole analyses)	$f_{m,N}$(Hz) (Nakajima model)	Ratio $f_{m,N}/f_{m,C-C}$
10	4.52×10^{-6}	2.76×10^{-5}	6.1
20	2.07×10^{-5}	4.73×10^{-5}	2.3
30	5.71×10^{-5}	8.10×10^{-5}	1.4
40	1.41×10^{-4}	1.11×10^{-4}	0.8

an increase in the electric field of the epoxy matrix. This increase causes the field in the epoxy matrix to the higher than it would be in the unfilled epoxy, because the dielectric constant of the filler for all of the materials used in the present study exceeds that of the epoxy; accordingly, the activation energies of the composites for both d.c. and a.c. conductions are less than that of the unfilled epoxy.

In the present study, the relaxation data have been obtained over a frequency range of 10^{-4}–10^{-1} Hz for the filled materials. Such data allow the current to be separated into a time-dependent (polarization) part and a d.c. conduction part. It is not unreasonable to assume that the electron transport and polarization processes in the filler particles are very fast, which would not take part in the low-frequency relaxation mechanism. Thus, it may be suggested that the low-frequency relaxation behaviour in this study is also ionic. Moreover, the observed height of the potential barrier for d.c., $\Delta H_{d.c.}$, is higher than that for a.c., $\Delta H_{a.c.}$, for each filled material, e.g. $\Delta H_{d.c.} = 3.78$ eV and $\Delta H_{a.c.} = 0.151$ eV for epoxy/40% ATD-6, which indicates the Taylor model holds for the filled materials. In other words, the addition of the fillers changes the distribution of potential barriers from the Nakajima model for the unfilled epoxy to the Taylor model for the filled epoxies. As yet it is not clear how this occurs. Intuitively, the "Maxwell–Wagner effect" [16], which plays a role in the electrical properties of the filled materials but does not play a role in those of the unfilled material, may be considered a factor. However, further study is needed to clarify this point.

5.3. Non-ohmic behaviour

We have found the conduction mechanisms for both unfilled and filled materials are ionic in a field level lower than 40 kV cm^{-1}, as suggested previously. We have also found that the non-linearity of the current density versus electric field plot is introduced at temperatures higher than 40 °C for the filled epoxies and 60 °C for the unfilled epoxy (see Figs 6–9). Because Equation 4 of the one-dimensional hopping model is non-linear in the electric field, it is of interest to see whether this non-linearity implies the occurrence of non-ionic conduction. At higher fields, the hyperbolic sine in Equation 4 can be expanded

$$\sinh\frac{eEa}{2kT} \simeq \frac{eEa}{2kT} + \frac{1}{3}\left(\frac{eEa}{2kT}\right)^3 \tag{20}$$

Substituting equation 20 in Equation 4, the current density, J, and the conductivity, σ, become

$$J \simeq \frac{ne^2a^2\nu_0E}{kT}\exp\left(\frac{-\Delta H}{kT}\right)\left(1+\frac{e^2a^2}{12k^2T^2}E^2\right) \tag{21}$$

and

$$\sigma = \frac{J}{E} \simeq \frac{ne^2a^2\nu_0}{kT}\exp\left(\frac{-\Delta H}{kT}\right)\left(1+\frac{e^2a^2}{12k^2T^2}E^2\right) \tag{22}$$

Thus, the plot of σ versus E^2 gives a linear relation at constant temperature. Such plots, shown in Figs 12–15,

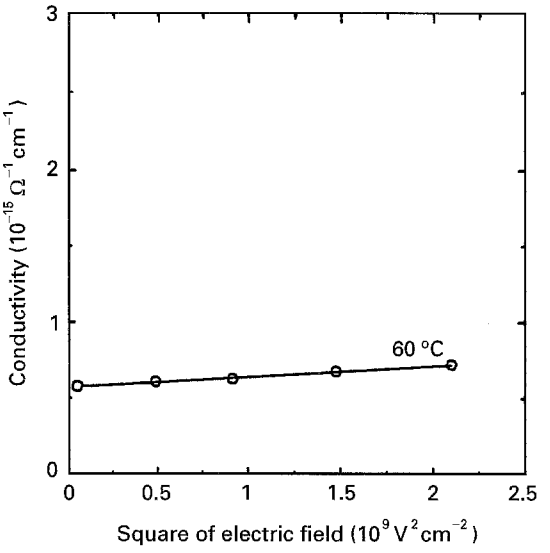

Figure 12 Conductivity versus square of electric field for unfilled epoxy at 60 °C.

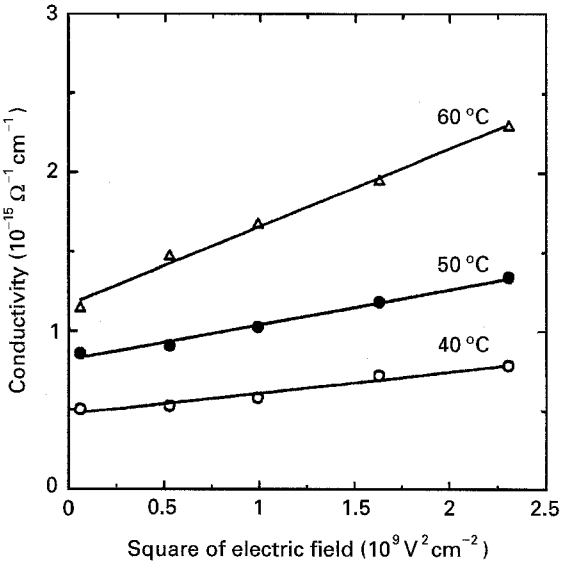

Figure 13 Conductivity versus square of electric field for epoxy/40% ATD-6 at temperatures 40–60 °C.

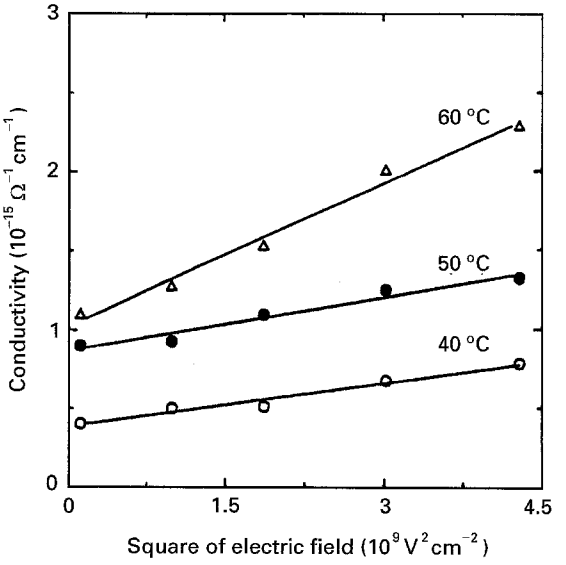

Figure 14 Conductivity versus square of electric field for epoxy/40% ATD-16 at temperatures 40–60 °C.

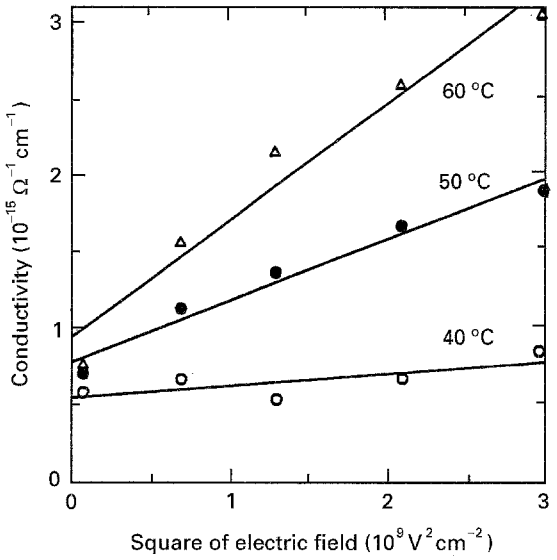

Figure 15 Conductivity versus square of electric field for epoxy/40% ATD-50 at temperatures 40–60 °C.

are found to be linear. For the limited range of data, the non-linearity found at the higher fields and temperatures could be fit with the simple model of ionic conduction based on the drift velocity expression of Equation 22.

6. Conclusion

The study has been directed toward identifying processes of conduction and polarization at low fields (lower than $6 \times 10^4\ V\,cm^{-1}$) and low frequencies ($10^{-4}$–$10^{-1}$ Hz) for the epoxy and its mineral-filled composites. It has been demonstrated that both polarization and conduction are ionic. For the unfilled epoxy, the distribution of potential barriers for ionic conduction could be fit by the Nakajima model, in which d.c. conduction and the polarization process involve the same activation energy. In contrast, the activation energies of the composites are considerably less for the polarization process than for d.c. conduction. This is consistent with the ionic hopping model proposed by Taylor, wherein ions can move over a region containing small potential barriers before being blocked by a large potential barrier. If the ion can overcome the large barriers, it takes part in d.c. conduction. However, if it can overcome the smaller but not the larger, it can only participate in a.c. conduction.

From the current density–electric field–temperature (J–E–T) characteristics, linear (ohmic) curves were observed for fields up to about $60\ kV\,cm^{-1}$ for temperatures up to about 20 °C. Then the current rose with increasing rapidity with further rise in temperature. For the limited range of data, those non-linear curves did not imply the occurrence of non-ionic conduction, but could be fit with the simple model of ionic conduction.

References

1. T. W. DARKIN, *IEEE Trans. Electric. Insul.* **9** (1974) 121.
2. R. H. ZEE, Y. H. HUANG, J. J. CHEN and B. Z. JANG, *Polym. Compos.* **10** (1989) 205.
3. S. L. WU and I.-C. TUNG, *ibid.* **16** (1995) 233.
4. M. IEDA, *IEEE Trans. Electric. Insul.* **19** (1984) 162.
5. J. J. O'DWYER, "The Theory of Conduction and Breakdown in Solid Dielectrics" (Clarendon Press, Oxford, 1973).
6. H. EYRING, *J. Chem. Phys.* **4** (1936) 283.
7. R. J. CHARLES, *J. Appl. Phys.* **32** (1961) 1115.
8. H. E. TAYLOR, *J. Soc. Glass Technol.* **43** (1959) 124T.
9. T. NAKAJIMA, *Ann. Rep. Conf. Electr. Insul. Dielectr. Phenom.* (1972) 168.
10. H. BLOCK, R. GROVES, P. W. LORD and S. M. WALKER, *J. Chem. Soc. Farad. Trans. II* **68** (1972) 1890.
11. W. YEH, Doctoral thesis, Auburn University (1990).
12. K. S. COLE and R. H. COLE, *J. Chem. Phys.* **9** (1941) 341.
13. R. A. FAVA and A. E. HORSFIELD, *J. Phys. D Appl. Phys.* **1** (1968) 117.
14. T. MIYAMOTO and K. SHIBAYAMA, *J. Appl. Phys.* **44**, (1973) 5372.
15. K. W. HANSEN and M. T. SPLANN, *J. Electrochem. Soc.* **113**, (1966) 895.
16. T. FURUKAWA and E. FUKADA, *Jpn. J. Appl. Phys.* **16** (1977) 453.

Received 3 June 1994
and accepted 8 September 1995